Journal of
Plankton Research

plankt.oxfordjournals.org

J. Plankton Res. (2016) 38(2): 199–215. First published online August 3, 2015 doi:10.1093/plankt/fbv063

Costa Rica Dome: Flux and Zinc Experiments

Phytoplankton production and taxon-specific growth rates in the Costa Rica Dome

KAREN E. SELPH[1]*, MICHAEL R. LANDRY[2], ANDREW G. TAYLOR[2], ANDRÉS GUTIÉRREZ-RODRÍGUEZ[2,3], MICHAEL R. STUKEL[4], JOHN WOKULUK[2] AND ALEXIS PASULKA[2,5]

[1]DEPARTMENT OF OCEANOGRAPHY, UNIVERSITY OF HAWAII AT MANOA, HONOLULU, HI 96822, USA, [2]SCRIPPS INSTITUTION OF OCEANOGRAPHY, 9500 GILMAN DR., LA JOLLA, CA 92093-0227, USA, [3]CENTRE NATIONAL DE LA RECHERCHE SCIENTIFIQUE AND UNIVERSITE PIERRE ET MARIE CURIE, STATION BIOLOGIQUE, 29680 ROSCOFF, FRANCE, [4]EARTH, OCEAN AND ATMOSPHERIC SCIENCE, FLORIDA STATE UNIVERSITY, TALLAHASSEE, FL 32306, USA AND [5]GEOLOGICAL AND PLANETARY SCIENCES, CALIFORNIA INSTITUTE OF TECHNOLOGY, PASADENA, CA 91125, USA

*CORRESPONDING AUTHOR: selph@hawaii.edu

Received April 11, 2015; accepted July 13, 2015

Corresponding editor: Pia Moisander

During summer 2010, we investigated phytoplankton production and growth rates at 19 stations in the eastern tropical Pacific, where winds and strong opposing currents generate the Costa Rica Dome (CRD), an open-ocean upwelling feature. Primary production (^{14}C-incorporation) and group-specific growth and net growth rates (two-treatment seawater dilution method) were estimated from samples incubated *in situ* at eight depths. Our cruise coincided with a mild El Niño event, and only weak upwelling was observed in the CRD. Nevertheless, the highest phytoplankton abundances were found near the dome center. However, mixed-layer growth rates were lowest in the dome center ($\sim$0.5–0.9 day^{-1}), but higher on the edge of the dome ($\sim$0.9–1.0 day^{-1}) and in adjacent coastal waters (0.9–1.3 day^{-1}). We found good agreement between independent methods to estimate growth rates. Mixed-layer growth rates of *Prochlorococcus* and *Synechococcus* were largely balanced by mortality, whereas eukaryotic phytoplankton showed positive net growth ($\sim$0.5–0.6 day^{-1}), that is, growth available to support larger (mesozooplankton) consumer biomass. These are the first group-specific phytoplankton rate estimates in this region, and they demonstrate that integrated primary production is high, exceeding 1 g C m^{-2} day^{-1} on average, even during a period of reduced upwelling.

KEYWORDS: phytoplankton; Costa Rica Dome; growth; mortality; microzooplankton

available online at www.plankt.oxfordjournals.org

INTRODUCTION

From satellite estimates of primary production, the Costa Rica Dome (CRD), a large (100–900 km) offshore upwelling area near 9°N, 90°W, is a productive region (Blackburn, 1966; Fiedler, 2002; Pennington *et al.*, 2006). Sampling since the late 1950–1960s has shown elevated concentrations of zooplankton there (Blackburn, 1966; Fiedler, 2002), including recent reports of large krill swarms (Matteson, 2009). It is therefore not surprising that important stocks of higher trophic level organisms congregate in or exploit resources in this area, such as squid paralarvae (Vecchione, 1999), yellowfin tuna (Shomura *et al.*, 1993), common dolphins (Au and Perryman, 1985; Fiedler, 2002; Ferguson *et al.*, 2006) and leatherback turtles (Shillinger *et al.*, 2008). Further, it is important as a nursery and feeding area for blue whales (Wade and Friedrichsen, 1979; Reilly and Thayer, 1990; Matteson, 2009). Thus, understanding the controls on phytoplankton productivity at the base of the food web is clearly of concern, especially as changing climate conditions might impact those processes and relationships upon which higher level organisms depend.

One current general paradigm associated with ocean productivity is that small picophytoplankton dominate in open-ocean oligotrophic regions and large microphytoplankton, particularly diatoms, dominate under upwelling and eutrophic conditions (e.g. for reviews, see Landry, 2002; Barber and Hiscock, 2006; Kudela *et al.*, 2008). In the CRD, however, the assemblage is dominated by picophytoplankton, including especially high abundances of *Synechococcus* (Li *et al.*, 1983; Saito *et al.*, 2005; Ahlgren *et al.*, 2014) as well as *Prochlorococcus* at concentrations typical for oligotrophic open-ocean sites (Saito *et al.*, 2005; Ahlgren *et al.*, 2014). Some evidence suggests that larger eukaryotic phytoplankton are limited by micronutrients in the CRD, such as the trace metals Co or Zn, likely in conjunction with silicate (Franck *et al.*, 2003; Saito *et al.*, 2005; Ahlgren *et al.*, 2014; Chappell *et al.*, 2016; Goes *et al.*, 2016; Krause *et al.*, 2016). However, most CRD studies have focused on *Synechococcus*, while the biomass, composition, growth and mortality of the full phytoplankton community of the region has received relatively little attention.

Here, we present phytoplankton community and group-specific growth and net growth rates from 19 stations in the CRD area sampled during June–July 2010. We used complementary independent methods to estimate growth rates, including seawater dilution experiments assessed for population and community rates by flow cytometry (FCM) and pigments, and rates determined from the combination of ^{14}C-primary production and community carbon biomass analyses from FCM and microscopy. Despite the fact that our cruise coincided with weak El Niño conditions, we measured high production and phytoplankton growth rates relatively broadly in the region. The data also show that while picophytoplankton comprise a major proportion of total biomass in the area, the larger eukaryotic phytoplankton grow fast and disproportionately escape grazing control by microzooplankton, forming the main food source and portion of primary production that is most efficiently transferred to mesozooplankton, and higher trophic levels.

METHOD

Sampling and experimental setup

Field sampling was conducted on the R/V Melville cruise MV1008 (22 June to 25 July 2010) in the CRD as part of the CRD Flux and Zinc Experiments project. We investigated phytoplankton dynamics and biogeochemical fluxes in five coherent multi-day cycles that were initiated at different starting locations in the CRD region, determined after a survey to locate the dome feature using acoustic Doppler current profiles (ADCP) and temperature data (Landry *et al.*, 2016a). A "cycle" includes multiple incubation profiles, each with experiments at eight depths. For each cycle, daily water-column sampling and *in situ* 24-h incubations were carried out for 4 days (3 days for Cycle 1) (Fig. 1), following a satellite-tracked drifter with a holey-sock drogue centered at 15 m (Landry *et al.*, 2009). A total of 19 incubation profiles were done on the cruise.

All samples for standing stock and rate determinations were collected from the early morning hydrocasts (~02:00 local time) within ~100 m of the drift array using Niskin bottles on a conductivity temperature depth (CTD) rosette. The Niskin water samples were collected at eight depths in the upper 80–100 m. Upper depths of 2, 12, 20 and generally 30 m were sampled on all profiles, with lower sampling depths differing to account for variability in chlorophyll fluorescence profiles observed.

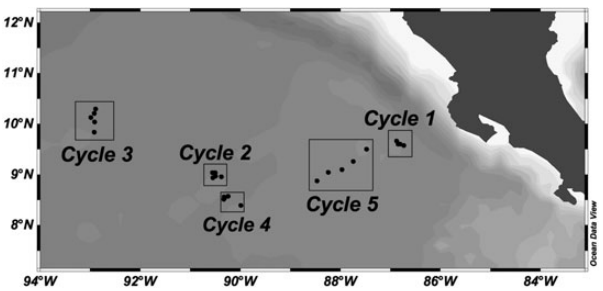

Fig. 1. Map of study region, showing station locations in each cycle (Cycles 1–5).

Samples for initial measurements of pigments and phytoplankton populations were filled directly from the Niskin bottles. Samples (50 mL) for macronutrient concentrations were first filtered through a 0.1-μm capsule filter (Suporcap). The nutrient sample tubes were rinsed three times with filtered seawater, and the filtrate was frozen (-18°C) for later analysis (within 2 months of collection).

For ^{14}C-uptake experiments (community net production), we filled two light and one dark bottle (250 mL, acid-cleaned polycarbonate) directly from the Niskin bottles and 100 μL of ^{14}C $NaHCO_3$ stock was added. For dilution experiments, we followed the two-treatment dilution approach (Landry *et al.*, 1984), as adapted to shipboard use (Landry *et al.*, 2008, 2011). This approach for estimating phytoplankton growth (μ_0) and mortality (m) at multiple depths in the euphotic zone assumes that microzooplankton feed at maximal rates *in situ* (e.g. maximal clearance rate F), and that dilution of ambient seawater results in a linear increase in net growth rate (k), as fewer grazers (G) translate to lower mortality rates (e.g. $m = F \times G$, and $k = \mu_0 - m$). To test the linearity assumption, we conducted a full-series dilution experiment (described below) in each cycle. For each sampling depth, a pair of polycarbonate bottles (2.7 L) were prepared; one of these contained unfiltered seawater (100%) and the second one had a 34:66 volumetric ratio of whole seawater and 0.1-μm filtered seawater, respectively, from the same depth. The seawater was filtered directly from the Niskin bottles using a peristaltic pump, silicone tubing and an in-line Suporcap filter capsule that had previously been acid washed (10% trace-metal grade HCl followed by Milli-Q and seawater rinses). Dilution treatment bottles first received pre-measured volumes of filtered seawater from the collection depths and were then gently filled (silicone tubing below the water level) with unscreened water from the Niskin bottles. After preparation, each bottle was subsampled for initial phytoplankton abundance by FCM and to confirm volumetric dilutions for other variables. No nutrients were added to these incubation bottles.

^{14}C-uptake and dilution bottles were placed into coarse net bags and clipped onto attached rings at the depth of collection on a line below the drift array float. The preparation process, from CTD arrival on deck to array deployment, was completed prior to local sunrise (within ~2 h). Upon recovery, ^{14}C-uptake samples were filtered onto 25-mm GF/F filters and placed in scintillation vials. Samples were acidified (1 mL of 10% HCl per sample) and allowed to sit, without a cap, at room temperature for at least 3 h before Ecolume cocktail (10 mL) was added. The vials were then counted on a Beckman 6100LC liquid scintillation counter (1.0% counting precision). The amount of carbon incorporated into the cells during the incubation (P) was calculated using standard methods (Strickland and Parsons, 1968). Upon array recovery, all dilution bottles were subsampled for final assessments of phytoplankton composition and biomass by FCM, taxon-specific accessory pigments and epifluorescence microscopy (EPI), as described further below.

To test the linearity assumptions of the dilution method (Landry and Hassett, 1982), we also conducted standard, multitreatment dilution experiments, one for each cycle, using water collected in the upper mixed layer, typically at 10 m, about an hour after local sunset (1900 CTD cast). Replicated dilution treatments of 0.22, 0.45, 0.65, 0.86 and 1.0× natural seawater were prepared in 2.2-L polycarbonate bottles as above, by adding measured aliquots of filtered water first. Each of these dilution treatment bottles received added nutrients (final concentrations of 0.5 μM nitrate, 0.03 μM phosphate) to promote constant phytoplankton growth. Two additional bottles were also prepared as replicate controls without added nutrients. Each of these bottles was filled with natural unscreened seawater from the depth of collection, from a mixing carboy that was filled gently via submerged tubing from the contents of several rosette bottles. All bottles were incubated for 24 h, starting ~2100 local time, in a surface seawater-cooled incubator screened to 31% of surface irradiance. We sampled each dilution bottle initially and at 24 h for FCM (1 mL). Triplicate initial Chl *a* samples (250 mL) were taken from the mixing carboy, and initial Chl *a* estimates in dilution bottles were computed volumetrically from the proportions of filtered and unfiltered water added (confirmed by FCM subsampling). Final Chl *a* samples were taken from each bottle.

Phytoplankton community analyses

To assess growth rates across a spectrum of phytoplankton taxonomic groups, we analyzed the community in initial and final seawater dilution samples using a combination of FCM, taxon-specific accessory pigments [high-pressure liquid chromatography (HPLC)] and EPI, all analyzed as described by Taylor *et al.* (Taylor *et al.*, 2016). Population abundances of picophytoplankton [*Prochlorococcus* (PRO), *Synechococcus* (SYN) and phototrophic pico-eukaryotes (PEUK)] were determined from 1 mL FCM samples, which were preserved (0.5% paraformaldehyde, v/v, final concentration) frozen in liquid nitrogen on shipboard, and stored at -80°C until analysis. Thawed samples were stained with Hoechst 33 342 (1 μg mL^{-1}, v/v, final concentration) at room temperature in the dark for 1 h (Monger and Landry, 1993). Aliquots (100 μL) were analyzed using a Beckman-Coulter EPICS Altra flow cytometer with a Harvard Apparatus syringe pump for volumetric sample delivery.

Simultaneous (co-linear) excitation of the plankton was provided by two water-cooled argon ion lasers, tuned to 488 nm (1 W) and the UV range (200 mW). The optical filter configuration distinguished populations on the basis of chlorophyll *a* (red fluorescence, 680 nm), phycoerythrin (orange fluorescence, 575 nm), DNA (blue fluorescence, 450 nm) and forward and 90° light scatter signatures. Calibration beads (0.5- and 1.0-μm yellow-green beads and 0.5-μm UV beads) were used as fluorescence standards. Raw data (listmode files) were processed using the software FlowJo (Treestar, Inc., www.flowjo.com). PRO and SYN abundance estimates from FCM analyses were converted to biomass using 32 and 101 fg C cell^{-1}, respectively (Garrison *et al.*, 2000; Brown *et al.*, 2008).

Concentrations of chlorophyll and carotenoid pigments were determined using HPLC. For HPLC analysis, 1.6–2.2-L samples of seawater were filtered onto Whatman GF/F filters, stored in liquid nitrogen and extracted in acetone as described by Goericke (Goericke, 2002). An internal standard (canthaxanthin) was added to the samples, which were analyzed on an Agilent 1100 series HPLC system (Agilent Technologies, Santa Clara, CA, USA) with a Waters Symmetry C8 column (3.5-μm particle size, 4.6 × 150 mm, silica, reverse-phase; Waters, Milford, MA, USA). Pigments were eluted using a gradient method with two solvents: (A) a mixture of methanol, acetonitrile and an aqueous pyridine solution (0.25 M, pH = 5) (50:25:25 v:v:v); and (B) a mixture of methanol, acetonitrile and acetone (20:60:20 v:v:v), according to the following times and mixtures (time, %A, %B): (0, 100, 0), (12, 60, 40), (36, 0, 100), (38, 0, 100), (40, 100, 0). Monovinyl Chl *a* (MVChl *a*) is found in SYN (prokaryote) and all eukaryotic phytoplankton. Divinyl Chl *a* (DVChl *a*) is only found in PRO. Accessory pigments are considered to identify the following groups, based on known pigment compositions (Wright and Jeffrey, 1987; Buma *et al.*, 1991; Vaulot *et al.*, 1994; Jeffrey and Vesk, 1997): fucoxanthin (FUCO) is found mainly in diatoms; 19′-hexanoyloxyfucoxanthin (HEX) has the highest concentration in prymnesiophytes; 19-butanoyloxyfucoxanthin (BUT) is highest in pelagophytes and peridinin (PER) is found in dinoflagellates, although absent in many species (e.g. Millie *et al.*, 1993).

Fluorometric chlorophyll *a* (Fluor-Chl *a*) was also analyzed using standard methods (Holm-Hansen *et al.*, 1965). Samples were filtered onto 25-mm Gelman GF/F filters and extracted in 10 mL of 90% acetone for 24 h at −20°C. Samples were analyzed with a Turner Designs model 10 fluorometer using equations calibrated against a pure chlorophyll *a* standard.

In the present study, we used initial and final biomass estimates from EPI from a subset of experiments ($n = 36$, mostly from Cycles 2–4) principally as an approach for assessing the mean net growth rates of dominant populations in the upper euphotic zone to compare against pigment-based estimates. For these analyses, seawater samples (500 mL) were preserved with 260 μL of alkaline Lugol's solution (0.56 M iodine, 0.86 M potassium iodide, 0.87 M sodium acetate), 10 mL 0.08 M borax-buffered 10% formalin and 500 μL 0.19 M sodium thiosulfate, gently mixing between each addition (Sherr and Sherr, 1993). After 1 h of fixation, the preserved samples were stained with 1 mL of proflavin (0.33% w/v) in the dark for another hour, then stained with 1 mL of 4′6-diamidino-2-phenylindole dihydrochloride (DAPI) (0.01 mg mL^{-1}) just prior to filtering. Subsamples of 50 mL were filtered onto 25-mm, black, 0.8-μm pore polycarbonate filters to enumerate smaller cells at ×630 magnification. The remaining 450 mL of sample were filtered onto 25-mm, black, 8.0-μm pore polycarbonate filters to count larger cells at ×200. Each filter was mounted onto a glass slide using immersion oil and a No. 2 cover slip. The slides were imaged and digitized using an automated Zeiss Axiovert 200 M inverted EPI, with a Zeiss AxioCam HRc color CCD digital camera (Taylor *et al.*, 2016). The following excitation/emission filter sets were used: fluorescein isothiocyanate (ex. 450–490 nm, em. 500–580 nm; Chl (ex. 465–495 nm, em. 635–685 nm) and DAPI (ex. 340–380 nm, em. 435–485 nm). Cell biovolumes (BV; μm^3) were determined from length (L) and width (W) measurements using the formula for a prolate sphere ($BV = 0.524\ L \times W^2$). Carbon (C; pg cell^{-1}) biomass of eukaryotic cells was computed from BV from the equations of Menden-Deuer and Lessard (Menden-Deuer and Lessard, 2000): $C = 0.216 \times BV^{0.939}$ for non-diatoms, and $C = 0.288 \times BV^{0.811}$ for diatoms. Phytoplankton carbon biomass (C) was estimated by the sum of all autotrophic biomass, e.g. eukaryotic biomass (calculated here), and PRO and SYN biomass (as described above).

Nutrient analysis

Nutrient samples were analyzed for nitrate, nitrite, ammonium, phosphate and silicate concentration by flow injection analysis at the nutrient laboratory of the University of California, Santa Barbara on a Lachat Instruments QuikChem 8000 using standard wet-chemistry methods (Gordon *et al.*, 1992). The precision of these measurements was ±5%, and the detection levels for nitrate + nitrite, nitrite, ammonium, phosphate and silicate were 0.2, 0.1, 0.1, 0.1 and 1.0 μM, respectively.

Rate determinations

We used multiple independent methods of determining rates, which are summarized for clarity in Table I. For

Table I: Equations used to estimate growth, net growth and mortality rates

Population	Measurement: FCM	HPLC	Chl	k = no nutrients and 100%WSW; k' = no nutrients and 34%WSW
A) 2-point dilution experiments[a]				
PRO, SYN, PEUK (*X*)	*X*			$k = 1/t \ln(X_f/X_i)$, $k' = 1/t \ln(X_f'/X_i')$
FUCO, HEX, BUT, PER (*Y*)		*X*		$k = 1/t \ln(Y_f/Y_i)$, $k' = 1/t \ln(Y_f'/Y_i')$
DVChl *a* (*D*)	*X*	*X*		$k = 1/t \ln(D_f/D_i) + k(\text{PRO}\Delta F)$, $k' = 1/t \ln(D_f'/D_i') + k(\text{PRO}\Delta F)$
MVChl *a* (*M*)	*X*	*X*		$k = 1/t \ln(M_f/M_i) + k(\text{SYN}\Delta F) + k(\text{PEU}K\Delta F)$, $k' = 1/t \ln(M_f'/M_i') + k(\text{SYN}\Delta F) + k(\text{PEU}K\Delta F)]$
TOTChl *a* (HPLC)	*X*	*X*		$k = 1/t\, k(\text{M}) + k(D)$, $k' = 1/t\, k'(M) + k'(D)$
Fluor-Chl *a* (Chl)	*X*		*X*	$k = k(\text{Chl}) + k(\text{PRO}\Delta F) + k(\text{SYN}\Delta F) + k(\text{PEU}K\Delta F)$, $k' = k'(\text{Chl}) + k(\text{PRO}\Delta F) + k(\text{SYN}\Delta F) + k(\text{PEU}K\Delta F)$
ΔChl *a*	*X*	*X*	*X*	$k(\text{FCM POP}\Delta F) = 1/t \ln(F_f/F_i)$
B) Full-series dilution experiments[b]				
POP	FCM	Chl	k_N = with nutrients, k_0 = no nutrients	
PRO, SYN, PEUK (*X*)	*X*		k_N or $k_0 = 1/t \ln(X_f/X_i)$	
Fluor-Chl *a* (FLUOR)		*X*	k_N or $k_0 = 1/t \ln(\text{FLUOR}_f/\text{FLUOR}_i)$	
C) ^{14}C-incorporation experiments[c]				
Parameter	FCM	EPI	μ (primary production incubations)	
Total phytoplankton community	*X*	*X*	$\mu^{14}\text{C} = 1/t \ln[(P + C_0)/C_0]$	

Populations were determined by flow cytometry (FCM), high-pressure liquid chromatography (HPLC) and epifluorescence microscopy (EPI). Total community autotrophic production was determined with rate estimates from fluorometric Chl *a* (Chl), HPLC Total Chl *a* (TOTChl *a*) and ^{14}C-incorporation. Details are described in the text. A) 2-point dilution experiments, B) Full-series dilution experiments and C) ^{14}C-incorporation experiments. Changes in chlorophyll per cell (PRO, SYN, PEUK) during the 24-h incubation (ΔChl *a*) are from FCM analyses of initial and final Chl *a* fluorescence (F_i and F_f, respectively). For ^{14}C-incorporation, the primary production (*P*) in the dark bottle was subtracted from the average of the light bottle values. PRO, *Prochlorococcus*; SYN, *Synechococcus*; PEUK, pico-eukaryotes; FUCO, fucoxanthin; HEX, hexfucoxanthin; BUT, butfucoxanthin; PER, peridinin; DVChl *a*, divinyl Chl *a*; MVChl *a*, monovinyl Chl *a*; AUTOBIOMASS, initial autotrophic biomass from FCM and EPI; CPM, count per minute, with subscripts: sample (S), blank (B) and total (T); *W*, weight of carbonate carbon in seawater (mg C m^{-3}) and *t*, incubation time (days).

[a]Equations: $\mu_0 = k + (k' - k)/(1 - D)$, where $D = 0.34$, $m = \mu_0 - k$.

[b]Equations: $\mu_0 = k_0 + m$; $\mu_N = k_N + m$; and $m = (\mu_N - k_N)/D$, where D (variable) = 22 – 100% WSW.

[c]Equations: P (mg C m^{-3} day^{-1}) = $[(\text{CPM}_S - \text{CPM}_B) \times W \times 1.05]/(\text{CPM}_T \times t)$; $C_0 = \sum$(AUTOBIOMASS).

the multitreatment dilution experiments, we computed daily instantaneous estimates of phytoplankton growth (μ, day^{-1}) and microzooplankton grazing rates (m, day^{-1}) for Fluor-Chl *a* and for FCM-measured populations (PRO, SYN, PEUK) by the standard linear regression and control treatment approach (Landry *et al.*, 1998). Growth rate with added nutrients (μ_n, intercept) and m (slope) were determined from the regression

$$k_n = \mu_n - (D \times m),$$

where k_n is the measured net growth rate in each bottle of the dilution series with added nutrients and D is the proportion of unfiltered seawater in the treatment. Ambient growth rate estimates without added nutrients (μ_o) were then determined by adding grazing estimates to the net growth rates (k) measured in bottles without added nutrients, $\mu_o = k + m$. The differences, if any, between μ_n and μ_o provide an indicator of the extent to which the rates are limited by the added nutrients (*N* and *P*).

From the two-bottle dilution experiments, we determined rate profiles for μ_o and k from each pair of incubated bottles and for each FCM or pigment-associated population of interest. Estimates of k were measured directly from incubations of the undiluted seawater. Estimates of μ_o were computed from

$$\mu_o = k + \frac{k' - k}{1 - D},$$

where k' is the measured net rate of change in the diluted treatment bottle (Landry *et al.*, 2008).

Pigment estimates of growth rates were corrected for bead-normalized red fluorescence from FCM to account for changes in cellular chlorophyll content during the 24-h incubations (Landry *et al.*, 2011). This correction is necessary to account for the response of phytoplankton to changes in ambient light or accidental addition of pigment-stimulating micronutrients during sample preparation. For each FCM category of PRO, SYN and PEUK, the analyses provided initial (i) and final (f) estimates of bead-normalized Chl *a* red fluorescence per cell (Fl), from which daily instantaneous rates of change for the 24-h incubations were computed as ln (Fl_f/Fl_i). We assigned the bead-normalized correction for PEUKs to all autotrophic eukaryotes (A-Euk). We used normalized

red-fluorescence changes for SYN and PEUK, adjusted for the relative contribution of each to their combined biomass, to derive corrections for the eukaryotic and prokaryotic autotrophs that contribute to MVChl *a*. Corrections for total Chl *a* were determined by the red-fluorescence corrections for PRO and combined SYN+PEUK, and their proportional contributions to TotChl *a* (= MVChl + DVChl *a*). The pigment corrections for eukaryotic phytoplankton (as well as for Chl *a*, in general) were similar on average and statistically indistinguishable for Cycles 2–5 (Fig. 2). In contrast, the pattern for Cycle 1 experiments was almost a mirror image. We consequently applied the same mean depth corrections to all of the Cycles 2–5 experiments and corrected for Cycle 1 separately.

Specific growth rates from the ^{14}C-incubation experiments (μ^{14}C) were estimated based on the *in situ* production rate (^{14}C incubation) and the initial microscopy-derived phytoplankton carbon biomass, using the following equation (Balch *et al.*, 2000):

$$\mu^{14}\mathrm{C} = \frac{1}{t}\ln\left[\frac{P + C_0}{C_0}\right]$$

where t is the incubation period (1 day), P is the change in carbon as measured with ^{14}C-incorporation, and C_0 is the initial phytoplankton carbon as determined by combined microscopy and FCM (Taylor *et al.*, 2016).

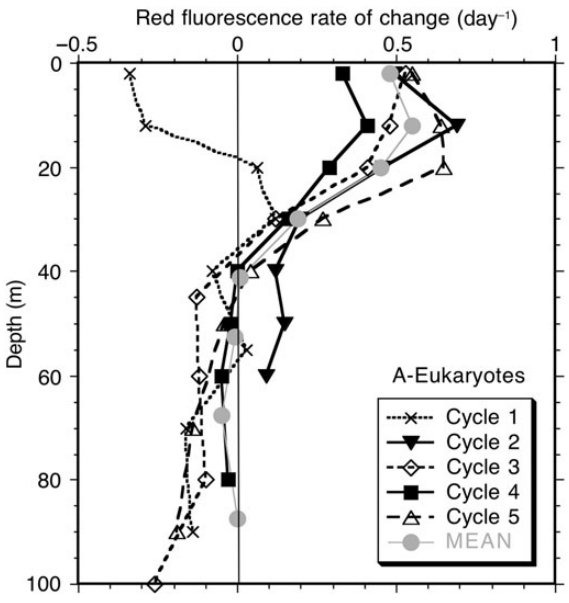

Fig. 2. Depth profiles of Chl *a* rate corrections for eukaryotic phytoplankton in the Costa Rica Dome. Corrections are median rates of change of bead-normalized cellular "red" fluorescence for Cycles 1–5 as determined from flow cytometric analyses of pigmented eukaryotic cells (A-Eukaryotes) in experimental bottles incubated for 24 h.

RESULTS

Study area

At the time of our study, conditions in the eastern tropical Pacific Ocean were changing from a weak El Niño to a weak La Niña (www.cpc.noaa.gov/products/analysis_monitoring/ensostuff/ensoyears.shtml). Surface expression of the dome was poorly defined by satellite images of temperature and chlorophyll *a* relative to normal summertime images (Landry *et al.*, 2016a), which suggests reduced upwelling and nutrient supply to CRD surface waters compared with typical summers. A transect survey through the area did however reveal isothermal shoaling of cooler and denser waters in the vicinity of the usual dome center (~9°N, 90°W), and this was chosen for study in Cycle 2 and visited later for Cycle 4 (Landry *et al.*, 2016a). An open-ocean site (Cycle 3) to the northwest was initially chosen to represent waters outside of the dome influence, but subsequent study of sea surface height image and density profiles suggest that this site was on the edge of the dynamic dome feature (Landry *et al.*, 2016a). Other experiments were conducted initially in southward-flowing waters close to the Costa Rica coast (Cycle 1) and at an open-ocean site to the east (Cycle 5) of the central dome area (Cycles 2 and 4). Since many supporting measurements such as ^{14}C production and phytoplankton community analyses were not made for Cycle 1 and since it was more coastal and different from the other sites, here we focus principally on experimental results from the open-ocean waters in and adjacent to the CRD (Cycles 2–5).

Physical and chemical environment

Average mixed-layer depths were very shallow, at ~10–20 m, as revealed by mean temperature (°C) and oxygen (mg L^{-1}) profiles for each cycle (Fig. 3). For Cycles 2 and 4, which were most influenced by weak upwelling, temperature declined sharply between 10 and 20 m (~5°C), especially when compared with the temperature profiles in the other cycles (<2°C). In all profiles, oxygen concentrations declined dramatically in the shallow thermocline to values about an order of magnitude lower at 40–50 m than at the surface. Depth distributions of macronutrients (nitrate, phosphate and silicate) showed the lowest concentrations in the mixed layer, increasing through the pycnocline, to high values at depth. Macronutrients were detectable in the mixed layer, with mean (±1 standard deviation) values of 1.46 ± 0.94 μM nitrate, 0.28 ± 0.07 μM phosphate and 2.38 ± 0.49 μM silicate. The dome cycles had the highest near-surface (0–12 m) concentrations of nitrate and silicate, at 1.6–3.9 μM nitrate and 2.8–4.2 μM silicate for Cycle 2 and 1.5–2.3 μM

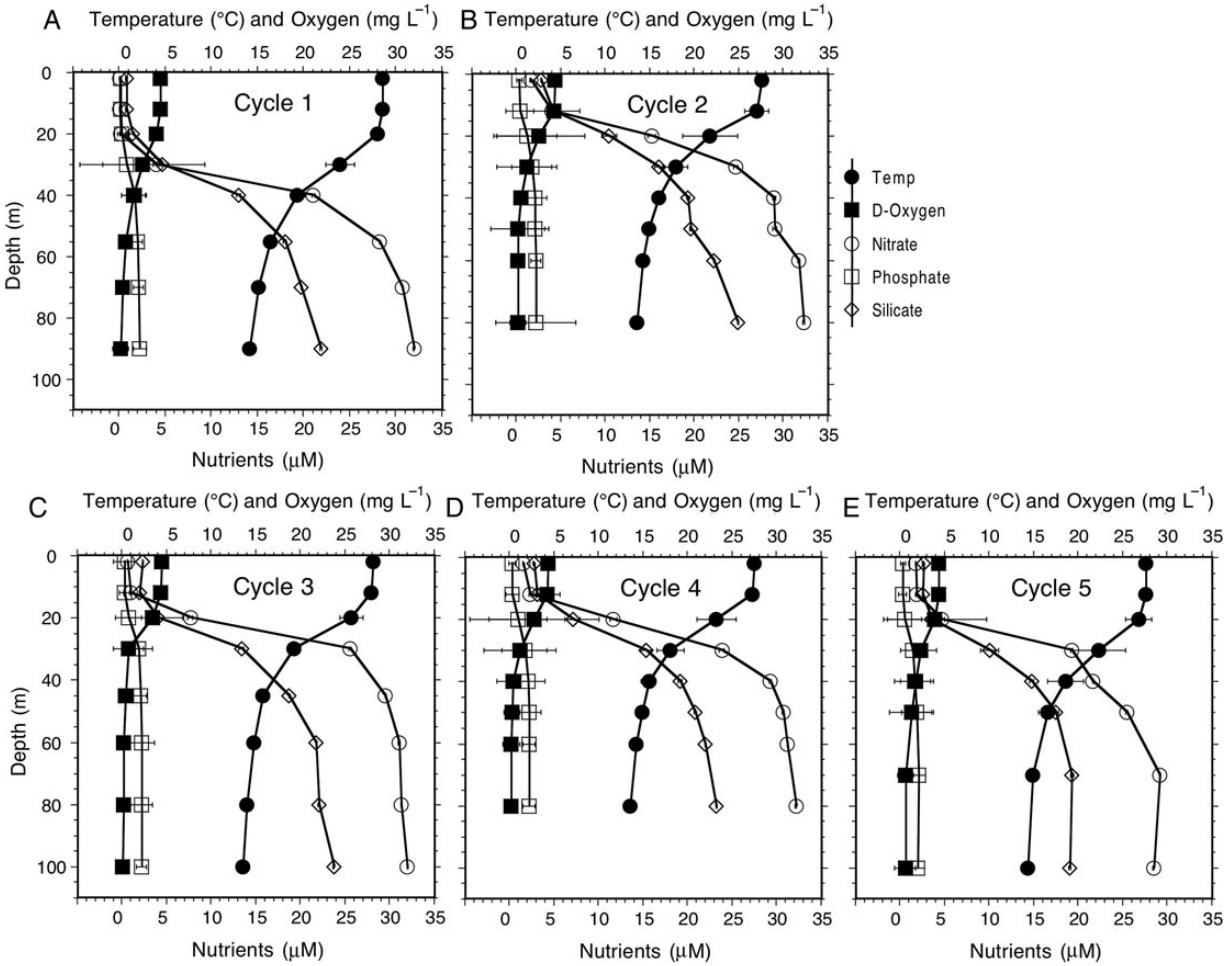

Fig. 3. Depth profiles of averages of temperature (°C), dissolved oxygen (D-Oxygen, mg L^{-1}) and macronutrient (nitrate, phosphate and silicate) concentrations (μM) during each cycle. (**A**) Cycle 1, (**B**) Cycle 2, (**C**) Cycle 3, (**D**) Cycle 4, (**E**) Cycle 5. Error estimates are ± 1 standard deviation for the mean values within each cycle.

nitrate and 2.7−3.1 μM silicate for Cycle 4. Nutrient concentrations for Cycle 5 were almost as high as the dome stations (1.7−1.8 μM nitrate and 2.5−2.6 μM silicate). Cycles 1 and 3 (coastal and offshore) had the lowest 0−12 m nitrate values at 0.06−0.08 and 0.6−1.0 μM nitrate, respectively. Silicate concentration was also lowest in surface waters of Cycle 1 and 3 (0.8 μM and 2.0−2.3 μM silicate, respectively).

Full dilution estimates of phytoplankton growth and mortality

Full dilution experiments conducted with mixed-layer water samples incubated at 31% of surface irradiance confirm that net measured growth rates during the experiments were linearly related to dilution factor, supporting application of the 2-point dilution method (Fig. 4). Cycle 1 analyses of Chl *a* were compromised; so these results are not included. The larger suite of rate estimates from the full dilution experiments are given in Table II. Chl *a* values were between 0.29 and 0.37 μg L^{-1} at the start of each experiment, with higher values near the dome upwelling center (Cycles 2 and 4). In contrast, community (Chl *a*) growth and grazing estimates were lowest in the central dome experiment (Cycle 2) and substantially higher for the other experiments (Cycles 3−5), and notably for Cycle 4, which was still in the central dome area. To our knowledge, there has only been one dilution experiment conducted previously in the central CRD area (Olson and Daly, 2013), and that gave growth and grazing estimates (0.47 and 0.51 day^{-1}, respectively) very similar to ours for Cycle 2 under similar environmental circumstances (50% PAR, 0.21 Chl *a* μg L^{-1}, 5.4 μM nitrate). Among the populations analyzed by FCM, abundances were generally higher and rates lower in the Cycle 2 experiment, except for

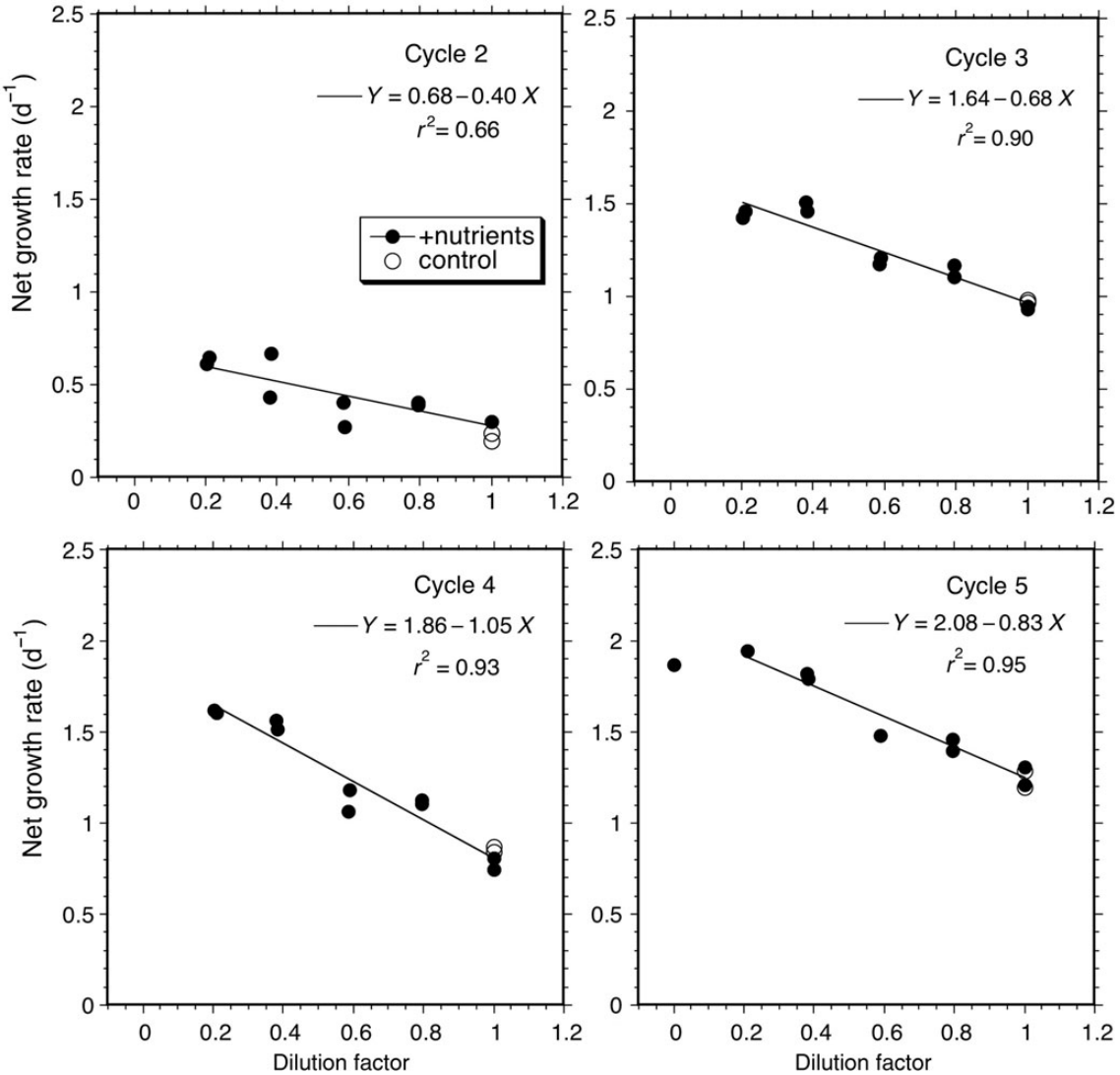

Fig. 4. Results of standard multitreatment dilution experiments conducted in shipboard incubations with mixed-layer water from Cycles 2–5. For nutrient-amended treatments (filled circles), regression equations give chlorophyll-based estimates of phytoplankton growth and microzooplankton grazing rates (day^{-1}) as the *Y*-intercepts and slopes, respectively. Open circle symbols are incubations without added nutrients.

PRO, which had high growth and comparably high grazing rates in the central dome area (Table II). Indeed, growth rate estimates for PRO in these experiments were higher than in daily *in situ* incubations (Fig. 5A), which we attribute to differences in the timing of the experiments relative to the post-sunset timing of PRO cell division. That is, the pre-sunrise setup of the *in situ* experiments provides a more reliable measure of growth rate over one photoperiod while the evening setup of the full dilution experiments overlaps and can confound the division cycles of two photoperiods.

While macronutrient-amendment (N and P) appears to give higher growth rate estimates (μ_n) than no-nutrient control bottles (μ_o) in experiments analyzed for Chl *a* (Table II), that was not the case for the raw Chl *a* readings, as illustrated by the similarity in net growth rates of nutrient and no-nutrient treatments in Fig. 4. The difference in Table II is that the μ_o values have been corrected for change in cellular pigment content not associated with phytoplankton biomass growth, but rather variations resulting from light or unintentional micronutrient changes. Systematic differences in nutrient versus no-nutrient growth rates were also not evident for analyses based on FCM cell counts (Table II). We conclude from these results that ambient concentrations of dissolved *N* and *P* in CRD surface waters during our cruise were not limiting to phytoplankton growth rate.

Table II: Concentrations, growth and grazing rates from full dilution experiments in the Costa Rica Dome

Variables	Cycle 1 26 June	Cycle 2 7 July	Cycle 3 12 July	Cycle 4 18 July	Cycle 5 23 July
Chl *a*		0.372	0.292	0.349	0.293
μ_n (day^{-1})		0.68	1.64	1.86	2.08
μ_o (day^{-1})		0.37	1.10	1.64	1.64
m (day^{-1})		0.40	0.68	1.05	0.84
r^2		0.66	0.90	0.93	0.96
PRO	58 100	100 000	78 200	90 100	47 600
μ_n (day^{-1})	1.49	1.24	1.18	1.02	0.78
μ_o (day^{-1})	1.18	1.22	1.27	1.05	0.81
m (day^{-1})	0.69	1.26	1.20	0.67	0.65
r^2	0.76	0.89	0.94	0.79	0.81
SYN	116 000	215 000	109 000	199 000	81 100
μ_n (day^{-1})	0.78	0.27	0.36	1.29	0.65
μ_o (day^{-1})	0.91	0.25	0.52	1.52	0.82
m (day^{-1})	0.60	0.83	0.55	1.34	0.46
r^2	0.86	0.81	0.61	0.93	0.71
PEUK	19 600	29 100	21 800	20 700	15 700
μ_n (day^{-1})	1.03	0.59	1.04	1.37	0.88
μ_o (day^{-1})	0.72	0.64	1.18	1.60	0.92
m (day^{-1})	0.66	0.71	0.60	1.30	0.52
r^2	0.81	0.85	0.89	0.94	0.81

Estimates are for the phytoplankton community (Chl *a*, μg L^{-1}), *Prochlorococcus* (PRO, cells mL^{-1}), *Synechococcus* (SYN, cells mL^{-1}) and photosynthetic eukaryotes (PEUK, cells mL^{-1}). Rates are instantaneous growth (μ_n) and grazing mortality (m) from linear regressions of the dilution series with nutrients (r^2 = correlation coefficient). μ_o is estimated growth rate from control incubations without nutrients, and including correction for net change in cellular pigment for Chl *a*. All experiments were conducted with mixed-layer water incubated in seawater-cooled deck incubators for 1 day at 31% of surface irradiance. Data for Chl *a*-based assessments in Cycle 1 are not available due to analytical problems.

Growth and net growth profiles of FCM populations

Among all cycles, depth-resolved daily growth (μ_o) and net growth (k) rates were indistinguishable within experimental error for PRO, SYN and PEUK populations (Fig. 5). Thus, the mean values for each population are plotted, along with their errors overlaying the individual cycle values. PRO and SYN showed largely balanced growth throughout the water column (i.e. growth = mortality; $k = 0$), whereas the PEUK populations showed net positive growth down to ~40 m.

In detail, PRO growth rates were positive, decreasing from the surface (~0.6 day^{-1}) to ~50 m (0.2 day^{-1}), and then were indistinguishable from zero at deeper depths (70 and 90 m) (Fig. 5A). Net PRO growth rates were essentially zero throughout the water column (Fig. 5D), indicating a close balance on average between growth and mortality attributable to microzooplankton grazers. Mean SYN growth rates were similar to PRO in the shallowest samples (surface and ~10 m at ~0.7 day^{-1}), but decreased with depth more rapidly than PRO (e.g. 0.3 day^{-1} at 20 m, decreasing to zero at 55 m) (Fig. 5B). Too few SYN were detected below 55 m to calculate meaningful growth rates at deeper depths. SYN net growth rates averaged zero at the surface, and were negative at the 10 and 20 m sample depths where grazing losses exceeded growth (Landry *et al.*, 2016b) (Fig. 5E). Below that, average net growth of SYN was indistinguishable from zero. PEUK growth rates were the highest, averaging ~1.0 day^{-1} at the surface and 10 m samples and decreasing gradually with depth to ~0.1 day^{-1} at 55 m (Fig. 5C). PEUK net growth rates averaged ~0.5 day^{-1} at the surface, and gradually decreased to zero at 40 m (Fig. 5F).

Community production and growth rates

For cycles with ^{14}C-uptake measurements of primary production (Cycles 2–5, 4 profiles each), the depth profiles show maximum rates at the surface, declining steadily with depth to about zero at ~60 m (Fig. 6A). Cycle 2 had the highest rates of surface productivity (70 ± 35 mg C m^{-3} day^{-1}) associated with high phytoplankton biomass in the central dome area. Maximum production rates in near-surface (2 m) incubations were lower and similar for Cycles 3–5 (~45 mg C m^{-3} day^{-1}). Depth-integrated mean primary production for the 16 depth profiles was 1077 ± 407 mg C m^{-2} day^{-1}.

Specific growth rates estimated from ^{14}C-primary production and community assessments of phytoplankton carbon biomass averaged ~0.9 ± 0.2 day^{-1} in surface waters decreasing gradually with depth (Fig. 6B). Near-surface specific growth rates were lowest in Cycle 2, intermediate in Cycle 4 and highest in Cycle 3. Only one profile was available in Cycle 5, due to lack of microscopy carbon estimates, so data from this cycle are omitted from Fig. 6B. On average, dilution estimates of specific growth rates for the phytoplankton community, assessed

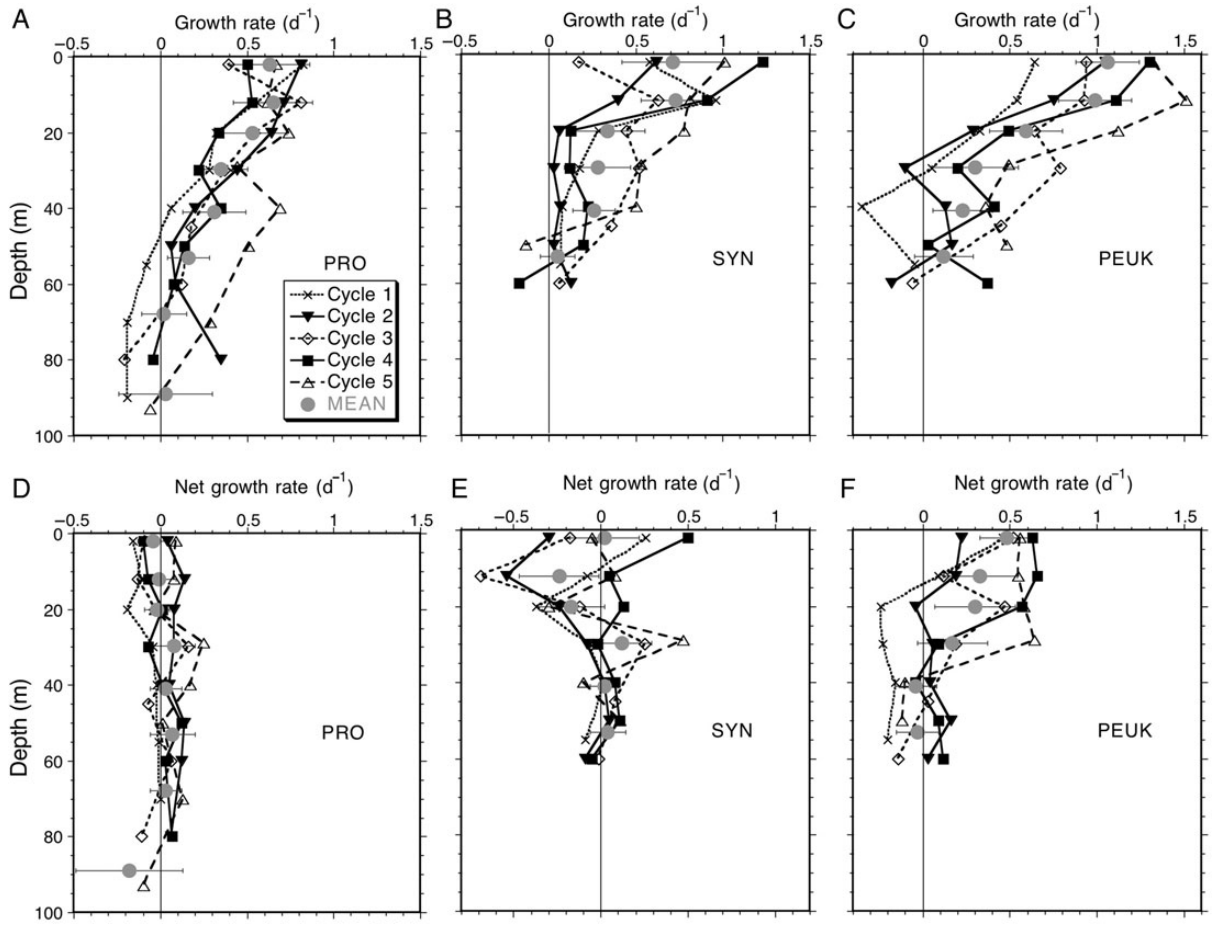

Fig. 5. Growth rate and net growth rate profiles from *in situ* dilution incubations in the Costa Rica Dome based on flow cytometrically determined cell counts of *Prochlorococcus* (PRO), *Synechococcus* (SYN) and photosynthetic pico-eukaryotes (PEUK) populations from Cycles 1–5. Growth and net growth rates of PRO (**A** and **D**), SYN (**B** and **E**) and PEUK (**C** and **F**), respectively. Error bars on mean estimates are 95% confidence intervals.

from fluorometric and HPLC analyses of Chl *a* corrected for net changes in cellular pigment, conformed closely to the rates and depth decline computed from ^{14}C and carbon biomass (Fig. 6C). The same pattern was also evident in independent analyses of PEUK by FCM (Fig. 6C). All methods suggest surface growth rates on the order 0.94–1.06 day^{-1}, decreasing gradually to zero in the upper 100 m. When just the upper 20 m (mixed-layer) samples are considered, average phytoplankton community growth rates were lowest for Cycle 2 and 4 experiments (~0.5–0.9 day^{-1}), and highest for Cycle 3 and 5 experiments (0.9–1.3 day^{-1}, Table III).

Group-specific growth rates based on pigment analyses

Depth profiles of growth rates for MVChl *a* varied considerably among cycles, with Cycle 2 consistently below and Cycle 5 consistently above the cruise means (Fig. 7A). On average, MVChl *a* growth rates were ~1.0 day^{-1} at the surface and decreased with depth to 0.2 day^{-1} at 40 m, and negligible values deeper (Fig. 7C). Individual cycle means showed significant positive rates extending deeper (Cycle 3), while others (Cycles 2 and 5) had negative rates below 40 m. Net growth rates for MVChl *a* were generally positive (0.5 day^{-1} on average) in surface incubations and decreased with depth to essentially zero at 40 m (Fig. 7B). Cycle 2 (center of dome) samples were notably different from the other cycles in having negligible to slightly negative net growth rates throughout the profile even at the shallowest depth.

Among group-specific pigments, most rate profiles varied similarly to MVChl *a*, mainly differing in magnitudes of near-surface estimates (Fig. 7C and D). For example, growth and net growth rates for FUCO (proxy for diatom biomass) were consistently higher than for other pigment-based rates, with surface maximum estimates of ~1.8 and 1.3 day^{-1}, respectively. Growth rates for HEX and BUT (indicative of prymnesiophytes and pelagophytes, respectively) were similar to each other and

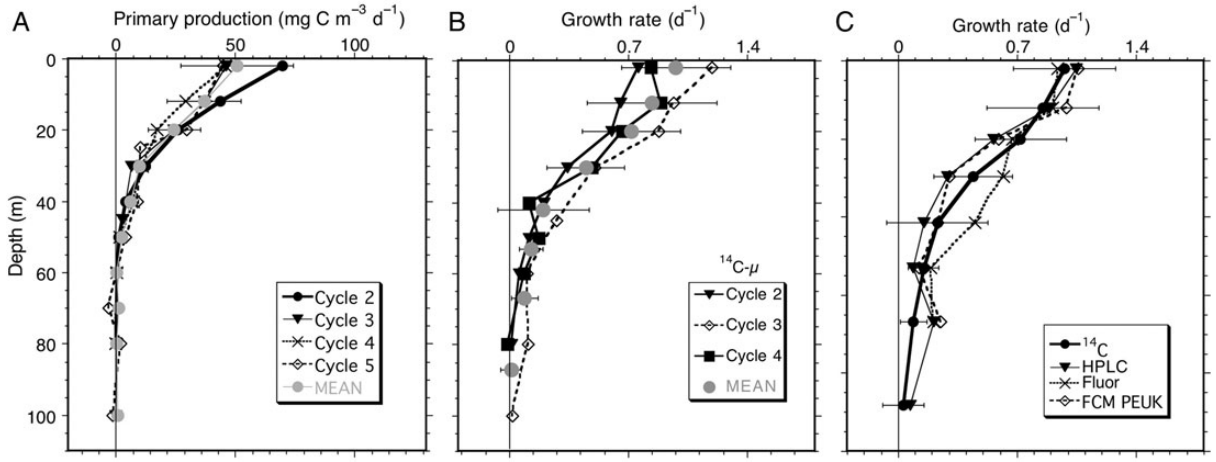

Fig. 6. Mean depth profiles of phytoplankton community production and specific growth rates in the Coast Rica Dome area, June–July 2010. (**A**) Primary production rates (mg C m^{-3} day^{-1}) from ^{14}C uptake. (**B**) Phytoplankton growth rates based on ^{14}C-incorporation and phytoplankton carbon biomass (Taylor *et al.*, 2016) for Cycles 2–4. Error estimates are ±1 standard deviation for all data means. (**C**) Comparison of phytoplankton growth rates (μ, day^{-1}) based on ^{14}C-primary production, Chl *a*- and cell-based dilution experiments. Dilution estimates are from fluorometric and HPLC assessments of total Chl *a*, after correction for net change of bead-normalized red fluorescence. ^{14}C-based growth rates are from independent incubations. Cell-based rates are from FCM counts of photosynthetic eukaryotes (PEUKS). All experiments were incubated *in situ*. Primary production measurements were not done for Cycle 1, and phytoplankton carbon biomass estimates are available for only one profile in Cycle 5.

Table III: Mean estimates of phytoplankton community growth rates (μ, day^{-1}) in the upper 20 m of the Costa Rica Dome based on ^{14}C-primary production (^{14}C-PrimProd) and Chl a*-based dilution experiments*

Variables	Cycle 2	Cycle 3	Cycle 4	Cycle 5
^{14}C-PrimProd	0.65 ± 0.26	1.01 ± 0.19	0.79 ± 0.44	0.92 ± 0.18
Dilution, HPLC	0.49 ± 0.29	0.97 ± 0.25	0.81 ± 0.27	1.27 ± 0.41
Dilution, Fluor	0.55 ± 0.30	0.94 ± 0.49	0.89 ± 0.34	1.26 ± 0.21
Experiments (*n*)	10	12	11	3

Dilution estimates are from fluorometric and HPLC assessments of total Chl *a*, after correction for net change of bead-normalized red fluorescence. ^{14}C-PrimProd estimates are independently determined from estimates of ^{14}C-uptake and phytoplankton carbon biomass from combined microscopy and flow cytometry (Taylor *et al.*, 2016). All experiments were incubated *in situ*. Three depths were routinely sampled in the upper 20 m of each profile, so with 16 profiles in Cycles 2–5, we ideally would report on 48 experiments. However, some bottles were lost on retrieval of the *in situ* array, so no estimates are available for two experiments in Cycle 2, and one experiment in Cycle 4. Also, no microscopy data are available for three of the four experiments in Cycle 5, so only three full comparisons could be made for these datasets. Thus, the total number of experiments compared is 36. Error estimates are ±1 standard deviation. *n*, number of experiments for the rate determinations.

to MVChl *a* throughout the euphotic zone, but net rates for BUT were generally higher than for HEX (Fig. 7D). Growth rates for PER, a dinoflagellate indicator, were also similar to the MVChl *a* means in shallow waters; however, the net rates hovered around zero. Rate assessments for PER were problematic due to low concentrations and could only be done for shallower depths at seven stations. They therefore do not provide an appropriate basis of comparison to the mean profiles for the other pigment-based rates for all stations.

DISCUSSION

We used the reduced two-treatment seawater dilution approach to generate rate profiles at eight depths per station. This approach was validated in each cycle for linearity of dilution response (Fig. 4). Perhaps due to the lack of pronounced upwelling in the CRD during our cruise, we did not find extreme variations in phytoplankton growth rates between experiments in and out of the dome; therefore, mean rate estimates at each depth describe phytoplankton growth dynamics for the region adequately. Nonetheless, it is intriguing that lower growth rate and higher biomass of phytoplankton occurred in the area that was nominally at the dome center (Cycle 2). Intuitively, these circumstances should occur downstream of open-ocean upwelling, where newly introduced nutrients to the euphotic zone first stimulate high growth rate at low biomass and only later lead to biomass accumulation. In the present case, this result could reflect the region's hydrographic complexity as well as the

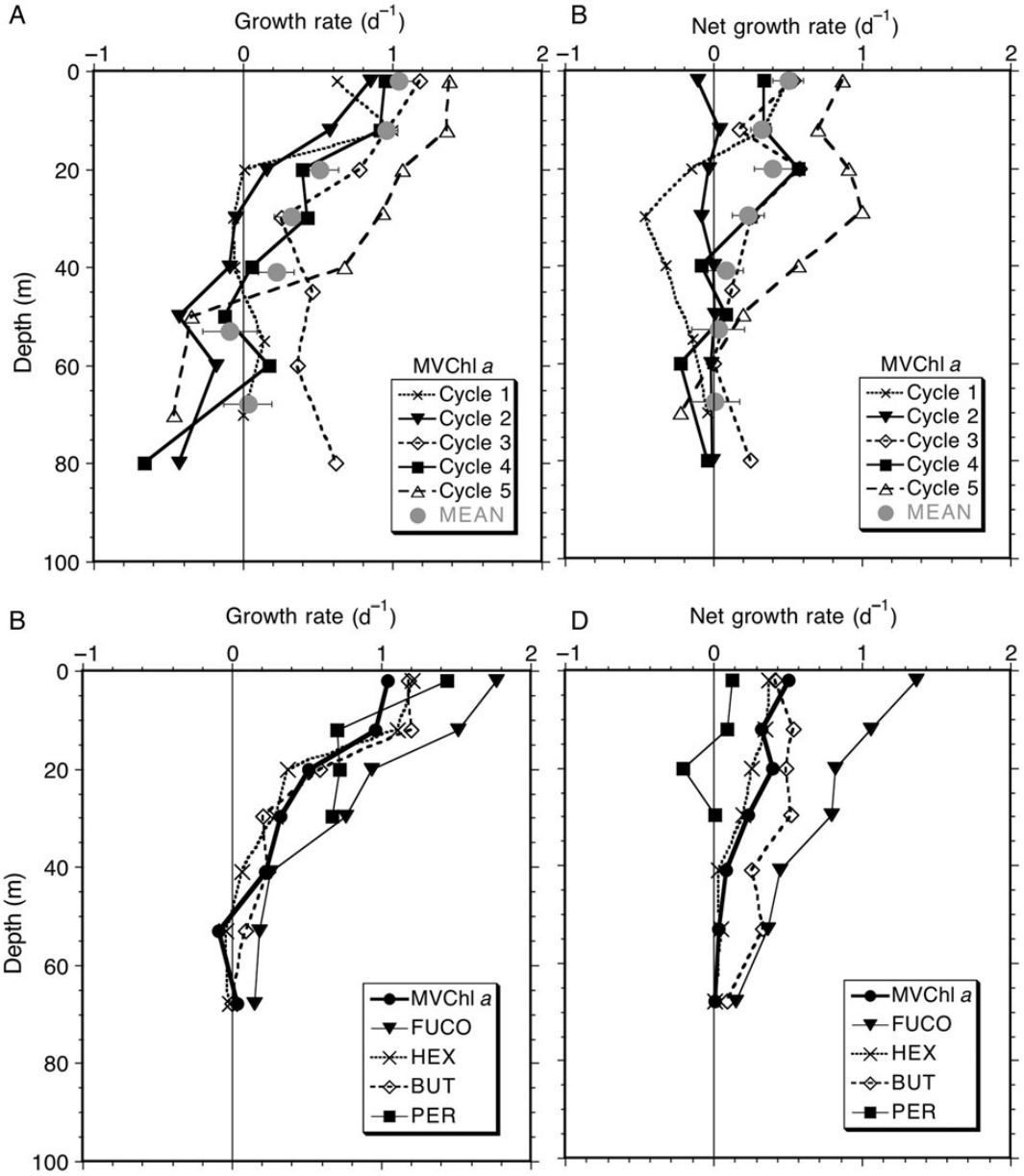

Fig. 7. Growth rate and net growth rate profiles from *in situ* dilution incubations in the Costa Rica Dome based on HPLC pigments. (**A**) Growth rates for MVChl *a* (pigment proxy for all phytoplankton except *Prochlorococcus*) from Cycles 1–5. Error estimates are ± 1 standard error for the mean values of all cycles. (**B**) Net growth rates for MVChl *a*. (**C**) Growth rates for major group-specific pigments. (**D**) Net growth rates for major pigments. For (**C** and **D**), MVChl *a* is the average for monovinyl Chl *a*. The remaining pigment estimates are indicative of mean rates for diatoms (FUCO), prymnesiophytes (HEX), pelagophytes (BUT) and dinoflagellates (PER).

uncertain histories and sources of the water parcels that we examined.

Among FCM-measured populations, PRO and SYN growth rates were balanced by microzooplankton grazing, but PEUK populations showed positive net growth (~0.5 day^{-1} in the surface mixed layer). Growth rates for MVChl *a* (a pigment present in all phytoplankton except PRO), HEX and BUT were similar to PEUK cell-based rates, indicative of a general eukaryote production surplus in excess of microzooplankton grazing. FUCO-based rates stand out as higher on average than all other groups, although the absolute percentage of diatom biomass to the phytoplankton community is very low (~2%, Taylor *et al.*, 2016). Overall, the high net growth rates of eukaryotic phytoplankton in the upper euphotic zone indicates that they are likely important in the diets of larger zooplankton grazers.

Dominant phytoplankton groups

As in previous studies of the CRD, SYN was a prominent member of the community, occurring at a high cell abundance (up to 2.8×10^5 cells mL^{-1}) and representing ~30% of the total phytoplankton biomass in Cycles 2 and 4, and ~18% of the biomass in Cycle 3 (Taylor *et al.*, 2016). We however did not encounter the very high SYN abundances of $>10^6$ cells mL^{-1} reported for previous cruises (Li *et al.*, 1983; Saito *et al.*, 2005; Ahlgren *et al.*, 2014). PRO was also present, with up to 2.8×10^5 cells mL^{-1}, and represented 11–22% of the biomass in Cycles 2, 3 and 4 (Taylor *et al.*, 2016). Most strikingly, the CRD differs from the other low-latitude HNLC area, the eastern Equatorial Pacific, where PRO exceeds SYN abundance by ~10-fold (e.g., Selph *et al.*, 2011). While it is not definitively known why SYN abundance is so high in the CRD, genetic work on the CRD cyanobacteria community during this project showed that phylogenetic diversity was high and included novel genotypes for both PRO and SYN, with strongly depth-stratified distributions in the central dome area (Gutiérrez-Rodríguez *et al.*, 2014).

For PRO, mixed-layer growth rates (0.6–0.7 day^{-1}) were similar to other areas of the equatorial Pacific (Landry *et al.*, 1995, 2003; Vaulot *et al.*, 1995, Binder *et al.*, 1996, Liu *et al.*, 1999, Selph *et al.*, 2011). However, perhaps due to the cloudy skies experienced during our cruise, there was no surface depression of PRO growth rates in the CRD as has been seen elsewhere (e.g., Selph *et al.*, 2011). SYN growth rates were more variable in the mixed layer but were similar, on average, to PRO, at ~0.7 day^{-1} (Fig. 5). The variability may have to do with different growth dynamics of SYN genotypes responding to subtle differences in habitat (Gutiérrez-Rodríguez *et al.*, 2014). Similarly, at Station ALOHA in the oligotrophic subtropical Pacific, SYN growth rates have been reported to be quite variable (Liu *et al.*, 1995), with a range of 0.17 ± 0.22 to 1.06 ± 0.18 day^{-1}. However, the average surface growth rate is similar to that found at the equator further to the west (Landry *et al.*, 1995; Selph *et al.*, 2011) and in the summer in the California Current (Worden and Binder, 2003).

Photosynthetic eukaryotes comprised a significant percentage of total phytoplankton biomass (48–71%, Taylor *et al.*, 2016) during our cruise. For the smaller size category analyzed here by FCM (nominally pico-eukaryotes, or PEUK), they tended to grow more rapidly, on average, than SYN or PRO (Fig. 5; Table II). The dominant PEUK groups were likely represented by the pigment signatures of HEX and BUT (i.e. prymnesiophytes and pelagophytes, respectively), the former being a recognizable component of the small cell assemblage in microscopical analyses (Taylor *et al.*, 2016).

Net growth rates of photosynthetic pico-eukaryote categories also generally exceeded those of SYN or PRO. Note that in Fig. 7C, the growth rate of MVChl *a* is on the low side of the group-specific eukaryote rates for FUCO, HEX, BUT and PER because MVChl *a* includes the slower average growth rate of SYN (~0.7 day^{-1}; Fig. 5). Thus, like the equatorial Pacific to the west, photosynthetic bacteria in the CRD appear to be regulated by a close growth-grazing balance by microzooplankton (Landry *et al.*, 1997; Barber and Hiscock, 2006). Similarly, while microzooplankton also graze on pico-, nano- and micro-eukaryotes, a significant fraction of their production (~40%) escapes micrograzer control.

Primary production comparison to other Pacific regions

We used normalized cellular red fluorescence from FCM analyses to adjust the pigment-based rates for changes in cellular pigment during the 24-h dilution incubation (Fig. 2). Although the surface pigment content increase observed may reflect unintended iron enrichment during water collection, such contamination would have negligible biomass or rate effects during 24-h incubations (Sanderson *et al.*, 1995; Landry *et al.*, 2000; MacIntyre *et al.*, 2000). Growth rates from this approach were also consistent with calculations based on measurements of primary production from ^{14}C-uptake and phytoplankton carbon biomass. Limited evidence from other projects that have compared ^{14}C-production-based growth rates with seawater dilution-based rates similarly have found good agreement (e.g. Chavez *et al.*, 1991; Landry *et al.*, 1997; LeBorgne and Landry, 2003). Future projects that do not have the capability to compare approaches may draw some support by the general agreement of these independent measurements.

When the available data are averaged (16 profiles), we estimate an integrated primary production rate of 1077 ± 407 mg C m^{-2} day^{-1}. This is significantly higher than the few other estimates of *in situ* primary production reported from the CRD area. For instance, Fiedler *et al.* (Fiedler *et al.*, 1991) reported higher phytoplankton productivity to the west of the dome (~700–800 mg C m^{-2} day^{-1}) than in the dome itself (~400 mg C m^{-2} day^{-1}) in August–November 1990. Pennington *et al.*'s (Pennington *et al.*, 2006) review of eastern tropical Pacific also gives low *in situ* primary production rates in the Gulf of Papagayo, which includes the CRD, of 365 mg C m^{-2} day^{-1}. In contrast, modeled estimates of productivity for the Gulf of Papagayo based on satellite (SeaWiFs) data average 997 mg C m^{-2} day^{-1} (Pennington *et al.*, 2006), close to our cruise mean. According to these researchers,

ship-collected data may be low as it includes lower productivity water from regions outside the CRD, whereas the model data include just the CRD.

Our primary production estimates are similar to or lower than coastal upwelling sites. For instance, Joint *et al.* (Joint *et al.*, 2001) reported a depth-integrated primary production maximum of 1053 mg C m^{-2} day^{-1} in the Iberian upwelling zone. Cervantes-Duarte *et al.* (Cervantes-Duarte *et al.*, 2015) report rates ranging from 930 to 1730 mg C m^{-2} day^{-1}, with an annual average of 1210 mg C m^{-2} day^{-1}, in the Southern Baja California coast upwelling area. In a coastal upwelling area of the East China Sea, integrated primary production ranged from 1470 to 4710 mg C m^{-2} day^{-1}, with the highest rates found at river outflow-influenced sites (Chen *et al.*, 2004). Other, generally higher, estimates of primary production from SeaWiFs-based satellite data are 1214, 3250, 2521 and 2427 mg C m^{-2} day^{-1} in the California (34–44°N), NW Africa (12–22°N), Peru (16–6°S) and Benguela (27.5–17.5°S) upwelling areas, respectively (Messié and Chavez, 2015). We note, however, that upwelling was not especially pronounced in the CRD during our cruise, and the abundance of SYN was lower than observed previously (Li *et al.*, 1983; Saito *et al.*, 2005; Ahlgren *et al.*, 2014). It is therefore possible, if not likely, that even higher primary production rates would be found in the CRD under "normal" summertime conditions.

Factors influencing growth rates in the CRD

In the present study, there was generally no significant correlation between light or temperature and group-specific growth rates, except perhaps light in Cycle 1 for surface photosynthetic pico-eukaryotes. Incident irradiance was much lower at Cycle 1 stations (~35 Ei cm^{-2} day^{-1}) relative to the other cycles (~50–60 Ei cm^{-2} day^{-1}) and Cycle 1 pico-eukaryotes had lower growth (~0.6 day^{-1}) compared with other cycles (>0.7 day^{-1}) (Fig. 5C).

It is still unclear what resource actually limits phytoplankton growth in the CRD. In more typical upwelling areas, nitrogen is accepted as the limiting growth nutrient. If we just consider the dome-influenced cycles (Cycle 2–4), we see no systematic enhancement of cell-based growth rates with macronutrient additions (Table II). However, in Cycle 1, which was conducted nearest to the coast with a surface concentration of 0.06 μM nitrate, PEUK and PRO did show some evidence of increased growth with added N and P. Overall, however, the dome-influenced cycles appear to be limited by resources other than nitrogen or phosphorus. In the main HNLC areas of the oceans, dissolved Fe is clearly the limiting resource (e.g. Martin *et al.*, 1990; Martin, 1992; Landry *et al.*, 1997; Boyd and Harrison, 1999). However, based on previous studies (Franck *et al.*, 2003; Saito *et al.*, 2005; Ahlgren *et al.*, 2014), including our own (Chappell *et al.*, 2016) which highlight the unique features of CRD phytoplankton, the growth limiting nutrient is likely a different trace metal or a combination of trace metals and silicate (Goes *et al.*, 2016).

If the limiting nutrient is a trace metal, it must be either provided to surface waters from below through upwelling or from above via dust deposition. One would expect growth rates to correlate with upwelling strength if the limiting nutrient is supplied through upwelling. If dust deposition is the main source, growth rates should correlate with the amount of dust deposited. From November through April, prevailing winds from the north north east (NNE) (Fiedler, 2002) could easily bring dust into the CRD system. During the rest of the year, the Inter Tropical Convergence Zone moves to the north, weakening the NNE wind jet, and the SE trade winds move northward (Fiedler, 2002); thus, less dust deposition would be expected. Saharan dust may even be deposited in the CRD by NNE winds, as models of the so-called Central American Dust Barrier have shown it to extend to 95°W at the latitude of the CRD (Nowottnick *et al.*, 2011). While aeolian dust inputs to the area and their trace-metal contents are poorly known, and unresolvable here, they may nonetheless be important at even low levels as new resource input to surface waters that help sustain high growth rates in waters advected away from the upwelling core of the dome.

Some insight into limiting resource responses can be derived by looking at growth rate patterns. While PRO growth rates were similar across the dome cycles (Cycles 2–4), indicative perhaps of its high competitive ability at very low nutrient concentrations, SYN and PEUK showed different growth and mortality patterns among the cycles (Table II). For instance, in Cycle 2, SYN and PEUK had their lowest growth rates and highest abundances, whereas in Cycle 4, their growth rates were much higher, while abundances were lower. Cycle 3 had intermediate growth rates between Cycles 2 and 4. The ratio of growth to mortality rates also differed among cycles. Cycle 2 had mortality rates greater than growth, whereas Cycle 4 showed the opposite pattern. Cycle 3 SYN growth rates were essentially equal to their mortality rates; however, PEUK growth rates greatly exceeded mortality.

How can we explain these patterns in growth? If we envision that phytoplankton consume the limiting nutrient and grow faster while the nutrient is still available, the population would accumulate biomass until grazing, other mortality agents, or advection acted in opposition. Thus, the imbalance between high growth and low

grazing in Cycle 4 suggests that the limiting nutrient was more newly available, while the relative balance between these processes in Cycle 3 might reflect a more advanced community state. In contrast, the low growth and high mortality rates during Cycle 2 suggest the aftermath of an earlier bloom for which the limiting nutrient has now been exhausted and phytoplankton biomass has overshot levels that can be sustained under balanced growth and grazing. In Cycle 2, Freibott *et al.* (Freibott *et al.*, 2016) found much higher abundances of heterotrophic dinoflagellates and ciliates relative to Cycle 3 and 4, supporting the high microzooplankton mortality finding here. Therefore, these growth/mortality patterns reasonably reflect different times since the limiting nutrient became available to the surface phytoplankton populations, perhaps in pulses of different intensity. Since their spatial relationships with respect to one another or to mean currents are not entirely coherent, they are best considered to represent temporally fragmented snapshots of the microbial community dynamics in the CRD.

In summary, even with relatively weak upwelling, we found the CRD to be a dynamic region, with high production and phytoplankton growth rates broadly distributed throughout the area (both in and out of the central region) and with unexpected variability in system state within the central region. The CRD contrasts with other upwelling regions, especially with its dominance of picophytoplankton and limitation of growth by micronutrients (e.g. a trace metal) as opposed to macronutrients; however, despite these characteristics, the CRD is as productive as other more "classical" upwelling areas. There is clearly more to learn about how delivery processes for the limiting trace element relates to the variability observed in microbial community dynamics, and ultimately to the resource habitat for high trophic levels in the region.

ACKNOWLEDGEMENTS

The authors thank Captain Christopher Curl, the crew, and resident technicians (Jim Dorrance, John Calderwood and Frank Delahoyde) aboard the *RV* Melville, for their excellent support of this research. They also thank the rest of the team that helped on board, in particular Darcy Taniguchi, Moira Décima and Alain de Verneil. This is contribution no. 9476 from the School of Ocean and Earth Science and Technology, University of Hawai'i at Manoa, Honolulu, HI 96822.

FUNDING

This study was supported by U.S. National Science Foundation grant OCE-0826626 to M.R.L. Additional support was provided by a Ramón Areces Foundation Fellowship to A.G.R., a NASA National Aeronautics and Space Administration, Earth and Space Science Fellowship to M.R.S. and a National Science Foundation Graduate Research Fellowship to A.L.P.

REFERENCES

Ahlgren, N. A., Noble, A., Patton, A. P., Roache-Johnson, K., Jackson, L., Robinson, D., McKay, C., Moore, L. R. *et al.* (2014) The unique trace metal and mixed layer conditions of the Costa Rica upwelling dome support a distinct and dense community of *Synechococcus*. *Limnol. Oceanogr.*, **59**, 2166–2184.

Au, D. W. K. and Perryman, W. L. (1985) Dolphin habitats in the eastern tropical Pacific. *Fish. Bull.*, **83**, 623–643.

Balch, W. M., Drapeau, D. T. and Fritz, J. J. (2000) Monsoonal forcing of calcification in the Arabian Sea. *Deep Sea Res. II*, **47**, 1301–1337.

Barber, R. T. and Hiscock, M. R. (2006) A rising tide lifts all phytoplankton: growth response of other phytoplankton taxa in diatom-dominated blooms. *Global Biogeochem. Cycles*, **20**, 1–12.

Binder, B. J., Chisholm, S. W., Olson, R. J., Frankel, S. L. and Worden, A. Z. (1996) Dynamics of picophytoplankton, ultraphytoplankton and bacteria in the central equatorial Pacific. *Deep Sea Res. II*, **43**, 907–931.

Blackburn, M. (1966) Relationships between standing crops at three successive trophic levels in the eastern tropical Pacific. *Pac. Sci.*, **20**, 36–59.

Boyd, P. and Harrison, P. J. (1999) Phytoplankton dynamics in the NE subarctic Pacific. *Deep Sea Res. II*, **46**, 2405–2432.

Brown, S. L., Landry, M. R., Selph, K. E., Yang, E. J., Rii, Y. M. and Bidigare, R. R. (2008) Diatoms in the desert; plankton community response to a mesoscale eddy in the subtropical North Pacific. *Deep Sea Res. II*, **55**, 1321–1333.

Buma, A. G. J., Bano, N., Veldhuis, M. J. W. and Kraay, G. W. (1991) Comparison of pigmentation of two strains of prymnesiophyte *Phaeocystis* sp. *Neth. J. Sea Res.*, **27**, 173–182.

Cervantes-Duarte, R., Prego, R., Gaxiola-Castro, G., López-López, S., Aguirre-Bahena, F. and Murillo-Murillo, I. (2015) Intra-annual upwelling patterns and its linkage with primary production in the euphotic zone (24.5°N) of Southern Baja California coast. *Estuarine Coastal Shelf Sci.*, **157**, 51–58.

Chappell, P. D., Vedmati, J., Selph, K. E., Cyr, H. A., Jenkins, B. D., Landry, M. R. and Moffett, J. W. (2016) Preferential depletion of zinc within the Costa Rica upwelling dome creates conditions for zinc co-limitation of primary production. *J. Plankton Res.* **38**, 244–255.

Chavez, F. P., Buck, K. R., Coale, K. H., Martin, J. H., DiTullio, G. R., Welschmeyer, N. A., Jacobson, A. C. and Barber, R. T. (1991) Growth rates, grazing, sinking and iron limitation of equatorial Pacific phytoplankton. *Limnol. Oceanogr.*, **36**, 1816–1833.

Chen, Y. L., Chen, H., Gong, G., Lin, Y., Jan, S. and Takahashi, M. (2004) Phytoplankton production during a summer coastal upwelling in the East China Sea. *Cont. Shelf Res.*, **24**, 1321–1338.

Ferguson, M. C., Barlow, J., Fiedler, P., Reilly, S. B. and Gerrodette, T. (2006) Spatial models of delphinid (family Delphinidae) encounter rate and group size in the eastern tropical Pacific Ocean. *Ecol. Model.*, **193**, 645–662.

Fiedler, P. C. (2002) The annual cycle and biological effects of the Costa Rica Dome. *Deep Sea Res. I*, **49**, 321–338.

Fiedler, P. C., Philbrick, V. and Chavez, F. P. (1991) Oceanic upwelling and productivity in the eastern tropical Pacific. *Limnol. Oceanogr.*, **36**, 1834–1850.

Franck, V. M., Bruland, K. W., Hutchins, D. A. and Brzezinski, M. A. (2003) Iron and zinc effects on silicic acid and nitrate uptake kinetics in three high-nutrient, low-chlorophyll (HNLC) regions. *Mar. Ecol. Prog. Ser.*, **252**, 15–33.

Freibott, A., Taylor, A. G., Selph, K. E., Liu, H., Zhang, W. and Landry, M. R. (2016) Biomass and composition of protist grazers and heterotrophic bacteria in the Costa Rica Dome during summer 2010. *J. Plankton Res.*, **38**, 230–243.

Garrison, D. L., Gowing, M. M., Hughes, M. P., Campbell, L., Caron, D. A., Dennett, M. R., Shalapyonok, A., Olson, R. J. *et al.* (2000) Microbial food web structure in the Arabian Sea: a US JGOFS study. *Deep Sea Res. II*, **47**, 1387–1422.

Goericke, R. (2002) Top-down control of phytoplankton biomass and community structure in the monsoonal Arabian Sea. *Limnol. Oceanogr.*, **47**, 1307–1323.

Goes, J. I., do Rosario, H., Selph, K. E. and Landry, M. R. (2016) Biological response of Costa Rica Dome phytoplankton to Light, Silicic acid and Trace metals. *J. Plankton Res.*, **38**, 290–304.

Gordon, L. I., Jennings, J. C., Ross, A. A. and Krest, J. M. (1992) A suggested protocol for continuous flow automated analysis of seawater nutrients in the WOCE hydrographic program and the Joint Global Ocean Fluxes Study. Grp. Tech Rpt 92–1, OSU College of Oceanography Descr. Chem Oc.

Gutiérrez-Rodríguez, A., Slack, G., Daniels, E., Selph, K. E., Palenik, B. and Landry, M. R. (2014) Fine spatial structure of genetically distinct picocyanobacterial populations across environmental gradients in the Costa Rica Dome. *Limnol. Oceanogr.*, **59**, 705–723.

Holm-Hansen, O., Lorenzen, C., Holmes, R. and Strickland, J. D. H. (1965) Fluorometric determination of chlorophyll. *J. Cons. Cons. Int. Explor. Mer*, **30**, 3–15.

Jeffrey, S. W. and Vesk, M. (1997) Introduction to marine phytoplankton and their pigment signatures. In: Jeffrey, S. W., Mantoura, R. C. F. and Wright, S. W. (eds), *Phytoplankton Pigments in Oceanography: Guidelines to Modern Methods*. UNESCO Publ., Paris, pp. 37–82.

Joint, I., Rees, A. P. and Woodward, M. S. (2001) Primary production and nutrient assimilation in the Iberian upwelling in August 1998. *Prog. Oceanogr.*, **51**, 303–320.

Krause, J. W., Stukel, M. R., Taylor, A. G., Taniguchi, D. A., De Verneil, A. and Landry, M. R. (2016) Net biogenic silica production and the contribution of diatoms to new production and organic matter export in the Costa Rica Dome ecosystem. *J. Plankton Res.*, **38**, 216–229.

Kudela, R. M., Banas, N. S., Barth, J. A., Frame, E. R., Jay, D. A., Largier, J. L., Lessard, E. J., Peterson, T. D. *et al.* (2008) New insights into the controls and mechanisms of plankton productivity in coastal upwelling waters of the northern California Current System. *Oceanography.*, **21**, 46–59.

Landry, M. R. (2002) Integrating classical and microbial food web concepts: evolving views from the open-ocean tropical Pacific. *Hydrobiologia*, **480**, 29–39.

Landry, M. R., Barber, R. T., Bidigare, R. R., Chai, F., Coale, K. H., Dam, H. G., Lewis, M. R., Lindley, S. T. *et al.* (1997) Iron and grazing constraints on primary production in the central equatorial Pacific: an EqPac synthesis. *Limnol. Oceanogr.*, **42**, 405–418.

Landry, M. R., Brown, S. L., Campbell, L., Constantinou, J. and Liu, H. (1998) Spatial patterns in phytoplankton growth and microzooplankton grazing in the Arabian Sea during monsoon forcing. *Deep Sea Res. II*, **45**, 2353–2368.

Landry, M. R., Brown, S. L., Neveux, J., Dupouy, C., Blanchot, J., Christensen, S. and Bidigare, R. R. (2003) Phytoplankton growth and microzooplankton grazing in HNLC waters of the equatorial Pacific: community and taxon-specific rate assessments from pigment and flow cytometric analyses. *J. Geophys. Res.*, **108**(C12), 8142.

Landry, M. L., Brown, S. L., Rii, Y. M., Selph, K. E., Bidigare, R. R., Yang, E. J. and Simmons, M. P. (2008) Depth-stratified phytoplankton dynamics in Cyclone *Opal*, a subtropical mesoscale eddy. *Deep Sea Res. II*, **55**, 1348–1359.

Landry, M. R., Constantinou, J. and Kirshtein, J. (1995) Microzooplankton grazing in the central equatorial Pacific during February and August, 1992. *Deep Sea Res. II*, **42**, 657–671.

Landry, M. R., Constantinou, J., Latasa, M., Brown, S. L., Bidigare, R. R. and Ondrusek, M. E. (2000) Biological response to iron fertilization in the eastern equatorial Pacific (IronEx II). III. Dynamics of phytoplankton growth and microzooplankton grazing. *Mar. Ecol. Prog Ser.*, **201**, 57–72.

Landry, M. R., Haas, L. W. and Fagerness, V. L. (1984) Dynamics of microplankton communities: experiments in Kaneohe Bay, Hawaii. *Mar. Ecol. Prog. Ser.*, **16**, 127–133.

Landry, M. R. and Hassett, R. P. (1982) Estimating the grazing impact of marine micro-zooplankton. *Mar. Biol.*, **67**, 283–288.

Landry, M. R., Ohman, M. D., Goericke, R., Stukel, M. R. and Tsyrklevich, K. (2009) Lagrangian studies of phytoplankton growth and grazing relationships in a coastal upwelling ecosystem off Southern California. *Prog. Oceanogr.*, **83**, 208–216.

Landry, M. R., de Verneil, A., Goes, J. I. and Moffett, J. W. (2016a) Plankton dynamics and biogeochemical fluxes in the Costa Rica Dome: introduction to the CRD Flux and Zinc Experiments. *J. Plankton Res.*, **38**, 167–182.

Landry, M. R., Selph, K. E., Décima, M., Gutiérrez-Rodríguez, A., Stukel, M. R., Taylor, A. G. and Pasulka, A. L. (2016b) Phytoplankton production and grazing balances in the Costa Rica Dome. *J. Plankton Res.*, **38**, 366–379.

Landry, M. R., Selph, K. E., Taylor, A. G., Décima, M., Balch, W. M. and Bidigare, R. R. (2011) Phytoplankton growth, grazing and production balances in the HNLC equatorial Pacific. *Deep Sea Res. II*, **58**, 524–535.

LeBorgne, R. and Landry, M. R. (2003) EBENE: a JGOFS investigation of plankton variability and trophic interactions in the equatorial Pacific (180°). *J. Geophys. Res.*, **108**, 8136.

Li, W. K. W., Subba Rao, D. V., Harrison, W. G., Smith, J. C., Cullen, J. J., Irwin, B. and Platt, T. (1983) Autotrophic picoplankton in the tropical ocean. *Science*, **219**, 292–295.

Liu, H., Campbell, L. and Landry, M. R. (1995) Growth and mortality rates of *Prochlorococcus* and *Synechococcus* measured with a selective inhibitor technique. *Mar. Ecol. Prog. Ser.*, **116**, 277–287.

Liu, H., Landry, M. R., Vaulot, D. and Campbell, L. (1999) *Prochlorococcus* growth rates in the central equatorial Pacific: an application of the fmax approach. *J. Geophys. Res.*, **117**(C2), 3391–3399.

MacIntyre, H. L., Kana, T. M. and Geider, R. J. (2000) The effect of water motion on short-term rates of photosynthesis by marine phytoplankton. *Trends. Plant. Sci.*, **5**, 12–17.

Martin, J. H. (1992) Iron as a limiting factor in oceanic productivity. In Falkowski, P. G. and Woodhead, A. D. (eds), *Primary Productivity and Biogeochemical Cycles in the Sea*. Plenum Press, New York, pp. 123–137.

Martin, J. H., Gordon, R. M. and Fitzwater, S. E. (1990) Iron in Antarctic waters. *Nature*, **345**, 156–158.

Matteson, R. S. (2009) The Costa Rica Dome: a study of physics, zooplankton and blue whales. Master's Thesis, Oregon State University.

Menden-Deuer, S. and Lessard, E. J. (2000) Carbon to volume relationships for dinoflagellates, diatoms, and other protist plankton. *Limnol. Oceanogr.*, **45**, 569–679.

Messié, M. and Chavez, F. P. (2015) Seasonal regulation of primary production in eastern boundary upwelling systems. *Progr. Oceanogr.* **134**, 1–18.

Millie, D. F., Paerl, H. W. and Hurley, J. P. (1993) Microalgal pigment assessments using high-performance liquid chromatography: a synopsis of organismal and ecological applications. *Can. J. Fish. Aquat. Sci.*, **50**, 2513–2527.

Monger, B. C. and Landry, M. R. (1993) Flow cytometric analysis of marine bacteria with Hoechst 33342. *Appl. Environ. Microbiol.*, **59**, 905–911.

Nowottnick, E., Colarco, P., da Silva, A., Hlavka, D. and McGill, M. (2011) The fate of Saharan dust across the Atlantic and implications for a central American dust barrier. *Atmos. Chem. Phys.*, **11**, 8415–8431.

Olson, M. B. and Daly, K. L. (2013) Micro-grazer biomass, composition and distribution across prey resource and dissolved oxygen gradients in the far eastern tropical north Pacific Ocean. *Deep Sea Res. I*, **75**, 28–38.

Pennington, J. T., Mahoney, K. L., Kuwahara, V. S., Kuwahara, V. S., Kolber, D. D., Calienes, R. and Chavez, F. P. (2006) Primary production in the eastern tropical Pacific: a review. *Prog. Oceanogr.*, **69**, 285–317.

Reilly, S. B. and Thayer, V. G. (1990) Blue whale (*Balaenoptera musculus*) distribution in the eastern tropical Pacific. *Mar. Mammal Sci.*, **6**, 265–277.

Saito, M. A., Rocap, G. and Moffett, J. W. (2005) Production of cobalt binding ligands in a *Synechococcus* feature at the Costa Rica upwelling dome. *Limnol. Oceanogr.*, **50**, 279–290.

Sanderson, M. P., Hunter, C. N., Fitzwater, S. E., Gordon, R. M. and Barber, R. T. (1995) Primary productivity and trace-metal contamination measurements from a clean rosette system versus ultra-clean Go-Flo bottles. *Deep Sea Res. II*, **42**, 431–440.

Selph, K. E., Landry, M. R., Taylor, A. G., Yang, E.-J., Measures, C. I., Yang, J., Stukel, M. R., Christensen, S. *et al.* (2011) Spatially-resolved taxon-specific phytoplankton production and grazing dynamics in relation to iron distributions in the Equatorial Pacific between 110 and 140°W. *Deep Sea Res. II*, **58**, 358–377.

Sherr, E. B. and Sherr, B. F. (1993) Preservation and storage of samples for enumeration of heterotrophic protists. In Kemp, P. K. *et al.* (eds), *Handbook of Methods in Aquatic Microbial Ecology.* CRC Press, Boca Raton, pp. 207–212.

Shillinger, G. L., Palacios, D. M., Bailey, H., Bograd, S. J., Swithenbank, A. M., Gaspar, P., Wallace, B. P., Spotilla, J. R. *et al.* (2008) Persistent leatherback turtle migrations present opportunities for conservation. *PLoS Biol.*, **6**, e171.

Shomura, R. S., Majkowski, J. and Langi, S. (1993) Interactions of Pacific tuna fisheries. Proceedings of the first FAO Expert Consultation on interactions of Pacific tuna fisheries. *FAO Fish. Tech. Pap.*, **336**, 439.

Strickland, J. D. H. and Parsons, T. R. (1968) A practical handbook of seawater analysis. *Bull. Fish. Res. Board Can.*, **167**, 293.

Taylor, A. G., Landry, M. R., Freibott, A., Selph, K. E. and Gutiérrez-Rodríguez, A. (2016) Patterns of microbial community biomass, composition and HPLC diagnostic pigments in the Costa Rica upwelling dome. *J. Plankton Res.*, **38**, 183–198.

Vaulot, D., Birrien, J.-L., Marie, D., Casotti, R., Veldhuis, M. J. W., Kraay, G. W. and Chrétiennot-Dinet, C. (1994) Morphology, ploidy, pigment composition and genome size of cultured strains of *Phaeocystis* (Prymnesiophyceae). *J. Phycol.*, **30**, 1022–1035.

Vaulot, D., Marie, D., Olson, R. J. and Chisholm, S. W. (1995) Growth of *Prochlorococcus*, a photosynthetic prokaryote, in the equatorial Pacific Ocean. *Science*, **268**, 1480–1482.

Vecchione, M. (1999) Extraordinary abundance of squid paralarvae in the tropical eastern Pacific Ocean during El Nino of 1987. *Fish. Bull.*, **97**, 1025–1030.

Wade, L. S. and Friedrichsen, G. L. (1979) Recent sightings of the blue whale, *Balenoptera musculus*, in the northeastern tropical Pacific. *Fish. Bull.*, **76**, 915–919.

Worden, A. Z. and Binder, B. J. (2003) Application of dilution experiments for measuring growth and mortality rates among *Prochlorococcus* and *Synechococcus* populations in oligotrophic environments. *Aquat. Microb. Ecol.*, **30**, 159–174.

Wright, S. W. and Jeffrey, S. W. (1987) Fucoxanthin pigment markers of marine phytoplankton analyzed by HPLC and HPTLC. *Mar. Ecol. Prog. Ser.*, **38**, 259–266.